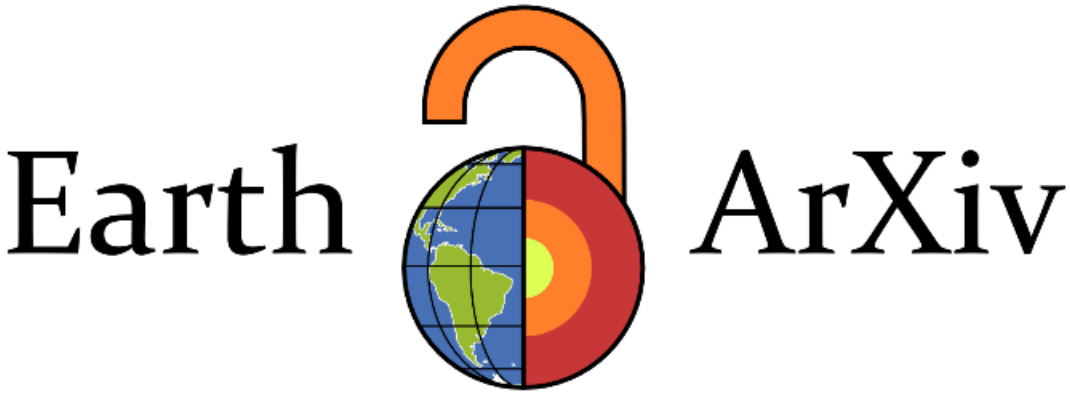

José Luis Abrego Salazar

Independent Researcher
La Paz – Bolivia
Email: joseluisabrego08@gmail.com
Cel: +59176502434

Microstructural Inference Framework for Saturated Soils Based on the Maximum Entropy Principle: Analytical Formulation, Numerical Implementation, and Validation

José Luis Abrego Salazar

Highlights

- Numerical-statistical finding: universal microstructural scaling law.
- Numerical-comparative finding: quantitative verification of tortuosity.
- New, objective inferential paradigm.
- Non-destructive, low-cost alternative.
- Honest and explicit limitation: unimodality and indistinguishability.

Abstract

The unit weight γ and the permeability k define an underdetermined inverse problem: infinitely many pore-size distributions $p(s)$ are compatible with the same pair of observations. Empirical correlations resolve this ambiguity by imposing rigid structural forms —valid only for a limited range of materials— that do not hold across the broad spectrum of natural soils.

This work formulates an inference framework based on Jaynes's Maximum Entropy Principle that selects, among all distributions compatible with γ and k, the one of maximum uncertainty, thereby avoiding unjustified assumptions. The exponential-canonical analytical solution is derived, existence and uniqueness are demonstrated through strict convexity, and a hybrid numerical engine verified by unit tests is implemented.

Validation over 2300 simulations spanning 23 reference soils reveals:

1. An invariant scaling law $Var[s] = a \cdot E[s]^b$ with $b = 2.0029 \pm 0.0227$ ($R^2 = 0.831$), robust to structural variations.

2. A systematic deviation from Poiseuille's law: an empirical slope of $E[s]$ vs. k of 0.186, against the theoretical value of 0.5, quantifying the effective tortuosity of the real medium through a correction factor $T \approx 50$.

The framework offers a non-destructive, low-cost alternative to destructive techniques such as MIP —with which a direct comparison is conceptually infeasible, since they operate in different state spaces— and provides an uncertainty filter to guide the use of more sophisticated tests. Its limitations —structural unimodality and the indistinguishability of microstructures with identical γ, k— are unavoidable consequences of the moment problem and are stated explicitly.

Keywords: Maximum Entropy; microstructural inference; permeability; unit weight; scaling laws; tortuosity.

1. Introduction

1.1. The inverse problem in soil characterization

Porous-media mechanics faces a **fundamental dichotomy** when characterizing a saturated soil. On one hand, macroscopic measurements are readily available through standardized laboratory tests: the bulk unit weight γ and the hydraulic permeability k. On the other hand, the physical behavior of the medium is governed by its internal architecture —the detailed pore-size distribution and its interconnection— a property that is not directly observable through routine tests.

In the sense of applied mathematics, this situation constitutes an **inverse problem**:

- **Forward problem:** Given the complete microstructure $p(s)$, the macroscopic response γ and k can be predicted. This is analytically straightforward.
- **Inverse problem:** Given γ_{obj} and k_{obj}, determine the internal microstructure $p(s)$. This is **inherently underdetermined**: an **infinite number** of pore-size distributions are compatible with exactly the same observed macroscopic properties.

The available data (γ, k) do not contain sufficient information to uniquely specify the material's internal structure. This ambiguity is not a technical limitation that could be corrected with more data of the same type; it is a **fundamental feature** of the physics of complex media.

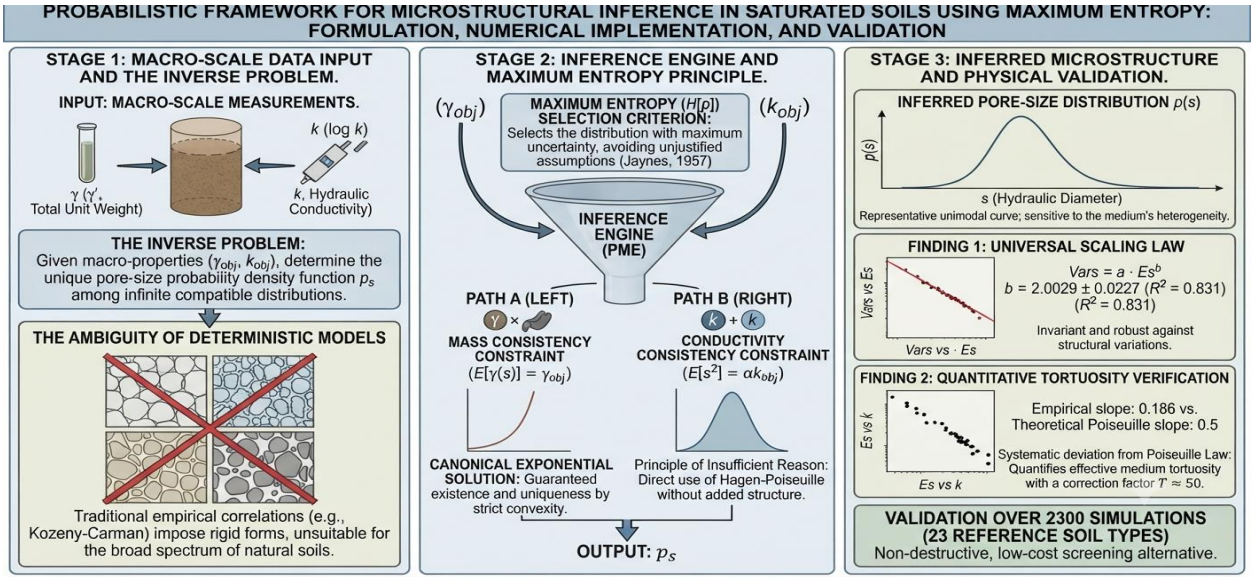

Fig. 1 — Conceptual scheme of the Maximum Entropy Principle (MEP) microstructural inference framework. The figure illustrates the three-stage workflow: (left) macroscopic input data (γ, k) and the underdetermined inverse problem; (center) the inference engine that maximizes Shannon entropy subject to mass and conductivity constraints; (right) the inferred pore-size distribution $p(s)$, from which two emergent findings arise.

1.2. Limitations of traditional empirical correlations

The dominant approach for circumventing this indeterminacy is to impose an empirical correlation between macroscopic variables. The paradigmatic example is the Kozeny–Carman equation, which relates the permeability k to the porosity n and a representative particle size D_{10} under the idealization of a bundle of parallel cylindrical capillaries.

The fundamental problem with this approach is that it assumes a rigid functional form for the relationship between k and pore size, based on an idealization of the medium that is rarely satisfied across the broad spectrum of natural soils. The Kozeny–Carman equation was calibrated essentially for clean, uniform sands; its application to clays, silts, or well-graded soils is, at best, a risky extrapolation. By defining empirical correlations, one is, *de facto*, assuming an underlying granular structure that may not be representative of reality. The result is a deterministic correlation model, not an inference model: it does not quantify the uncertainty associated with the indeterminacy of the inverse problem, but instead resolves it arbitrarily through an unverified structural choice.

1.3. The Maximum Entropy Principle as a criterion for objective inference

The Maximum Entropy Principle (MEP), formulated by Jaynes (1957), offers an epistemologically distinct alternative. Faced with the impossibility of knowing the microstructure with certainty, the MEP provides a rational and logically consistent criterion for selecting a unique probability distribution, based exclusively on the available information and avoiding the introduction of unverified assumptions.

In essence, the MEP formalizes Laplace's principle of insufficient reason: when there is no information favoring one possibility over another, equal probability should be assigned to all of them. When extended to systems with partial information, it becomes a method of objective selection that:

1. **Maximizes uncertainty** (or, equivalently, introduces the minimum additional information not contained in the constraints).

2. **Does not impose** a structural form (such as uniformity, normality, or the Kozeny–Carman form).

3. **Infers** the structure from the available data, rather than assuming it.

This formalism is the foundation of **statistical mechanics** and, by extension, of information theory as applied to the characterization of complex media.

1.4. Why is this framework needed now? The absence of a non-destructive benchmark

At present, there is no non-destructive reference method for characterizing the microstructure of a soil in situ or in intact samples that could serve as a benchmark for this type of inferential model.

The available techniques present fundamental limitations:

- **Mercury intrusion porosimetry (MIP):**
  - Performed on altered samples (dried, fragmented, or prepared).
  - Destroys the microstructure during high-pressure intrusion.
  - Does not fill all voids: the smallest or isolated pores may not be accessible to mercury.
  - Measures the volume of pores intruded under pressure, not a probability density of hydraulic diameter.
  - Is costly, destructive, and not reproducible on the same sample.
- **Tomography (micro-CT, nano-tomography):**
  - Is intrusive (requires large equipment and, often, synchrotrons).
  - Has resolution and sample-size limitations.
  - Is extremely costly and unavailable in routine practice.
- **Electron microscopy (SEM, TEM):**
  - Requires extensive sample preparation (dehydration, sectioning, metallization).
  - Is destructive and localized (does not represent the full volume).

The only data source available for validating a model of this kind is therefore the canonical geotechnical literature, which provides ranges of γ and k for different soil types. Validation of the framework is not conceived as a geometric comparison with MIP —which operates in a different state space— but rather as a check of thermodynamic and predictive consistency against the canonical geotechnical literature.

This limitation is not a weakness of the model; it is an honest acknowledgment of the state of the art. The MEP framework does not aim to replace direct measurement, but rather to provide an objective preliminary characterization and an uncertainty filter that indicates when more sophisticated tests are warranted. It is a screening tool that, from two routine tests, allows one to decide whether it is worth investing in a detailed microstructural characterization.

1.5. Contribution and structure of the article

The present work contributes:

1. A complete analytical formulation of the microstructural inference problem under the MEP, including the explicit construction of the physical bridge between micro- and macroscopic variables, and a rigorous proof of existence and uniqueness of the solution.

2. A stable numerical implementation verified through unit tests, which solves the associated nonlinear consistency system with a robust hybrid engine.

3. Extensive validation across 23 soil types representative of the canonical geotechnical literature, demonstrating the robustness and physical consistency of the proposed framework, including the discovery of an emergent scaling law and an intrinsic thermodynamic classification.

The remainder of the article is organized as follows: Section 2 develops the theoretical formulation; Section 3 describes the numerical solution strategy; Section 4 presents the validation results; Section 5 discusses the implications, limitations, and typical objections to the

model —including the difficulty of measuring tortuosity experimentally—; and Section 6 summarizes the conclusions and directions for future work.

2. Theoretical formulation of the inference model

2.1. State space and measure of uncertainty

2.1.1. Definition of pore size and its physical domain

The state variable s is defined as the **hydraulic diameter** of the pores, a generalization of the classical fluid-mechanics definition (four times the ratio of pore volume to wetted surface area). The physical domain of s is defined as the compact interval:

$$\mathcal{S} = [s_{\min}, s_{\max}] \subset \mathbb{R}^{+}$$

where $s_{\min} \geq 0$ reflects the limit imposed by particle size and packing density, and $s_{\max} < \infty$ reflects the size of the largest pores that can exist within the granular skeleton of the medium, while also ensuring the integrability of all functions in the model.

2.1.2. Probability density function and Shannon entropy

Uncertainty about the microstructure is represented by a probability density function $p(s)$, subject to the conditions of non-negativity and normalization:

$$p(s) \geq 0, \quad \forall s \in \mathcal{S}$$

$$\int_{s_{\min}}^{s_{\max}} p\,(s)\, ds = 1$$

The measure of uncertainty associated with $p(s)$ is the **Shannon entropy** (or differential entropy):

$$H[p] = -\int_{s_{\min}}^{s_{\max}} p\,(s) \ln p(s)\, ds$$

In the geotechnical context, $H[p]$ admits a direct physical interpretation as a quantitative measure of the structural heterogeneity of the medium:

- **Low entropy** → relatively **uniform** microstructure ($p(s)$ concentrated around a dominant size) → well-sorted or uniformly graded soil.
- **High entropy** → **heterogeneous** microstructure ($p(s)$ broad and dispersed over the domain) → poorly-sorted soil, with a mixture of fine and coarse fractions.

Unlike variance, entropy captures the **overall dispersion** of the distribution without privileging any particular value, and is sensitive even to multimodal shapes —although, as discussed in Section 5.4.2, the current model cannot resolve bimodality without additional constraints.

2.1.3. Justification for the choice of the Lebesgue measure ds

The parametrization of s in centimeters —its natural scale in soil mechanics— justifies maximizing the differential entropy defined with respect to the **Lebesgue measure** ds, rather than an alternative measure such as ds/s (Jeffreys's prior), which would favor logarithmic scales *a priori* without such a preference being justified by the available information.

Adopting ds/s would amount to introducing an informative prior not contained in the macroscopic constraints of the problem, violating the principle of epistemic conservatism underlying the MEP. The choice of ds is therefore the minimum-structure option consistent with the natural physical parametrization of the problem.

2.2. Macroscopic constraints (available information)

2.2.1. Mass constraint (bulk unit weight)

The first constraint requires that the expected value of the microscopic unit weight $\gamma(s)$ —a function derived in Section 2.3.2— match the experimentally measured unit weight:

$$E[\gamma(s)] = \int \gamma(s)\, p(s)\, ds = \gamma_{\text{obj}}$$

This constraint ensures **conservation of total mass** in the system: any distribution $p(s)$ that does not satisfy it would be physically inconsistent with the density measured in the laboratory.

2.2.2. Conductivity constraint (permeability)

The second constraint is derived from **Poiseuille's law**, which establishes the proportionality between the hydraulic conductivity of a capillary and the square of its diameter:

$$E[s^2] = \int s^2\, p(s)\, ds = \alpha\, k_{\text{obj}}$$

where $\alpha = 32\mu/(\gamma_w g)$ is the Hagen–Poiseuille constant, which groups together the fluid's dynamic viscosity μ, its density γ_w, and gravitational acceleration g.

Unlike the mass constraint, this is a simple second-order statistical moment of the state variable s itself, and captures the characteristic pore scale that governs flow.

2.3. Micro–macro physical bridge (minimum structure)

2.3.1. Auxiliary porosity $n(s)$

To connect $\gamma(s)$ to the intrinsic densities of the solid and liquid phases, an auxiliary porosity relation is introduced —not an independent constraint of the optimization problem, since this would overdetermine the system with three equations for only two multipliers.

Through a **first-order Taylor expansion** in the logarithmic variable $x \equiv ln(s/s_0)$, truncated precisely at the lowest non-trivial order compatible with a monotonic trend, one obtains:

$$n(s) = n_0 + \beta \ln(s/s_0)$$

The logarithmic form reflects the scale invariance of pore size (which spans several orders of magnitude in natural soils), and constitutes the minimum-structure choice justifiable without

introducing curvature or asymptotic behavior unsupported by observations. The sign $\beta > 0$ is adopted as a physical assumption: large pores are associated with a more open packing (higher local porosity).

2.3.2. Unit weight function $\gamma(s)$

From the **phase equilibrium** of a two-component saturated medium (solid and water, under the condition $S_r = 100\%$), the unit weight of a representative elementary volume is:

$$\gamma(s) = \gamma_s \left(1 - n(s)\right) + \gamma_w \, n(s)$$

Substituting $n(s)$ and defining $\Delta\gamma \equiv \gamma_s - \gamma_w$ (positive for virtually all mineral soils, since $\gamma_s > \gamma_w$), the closed form is obtained:

$$\gamma(s) = (\gamma_s - n_0 \Delta\gamma) - \beta \Delta\gamma \ln(s/s_0)$$

Differentiating with respect to s shows that:

$$\frac{d\gamma}{ds} = -\frac{\beta \Delta\gamma}{s} < 0 \quad \forall s \in \mathcal{S}$$

(since $s > 0$, $\Delta\gamma > 0$, and $\beta > 0$), so that $\gamma(s)$ is **strictly decreasing**: elements dominated by large pores have a lower unit weight, consistent with the physics of loose and dense soils.

2.3.3. Permeability function $k(s)$

From the **Hagen–Poiseuille equation** for laminar flow in a cylindrical conduit, and the standard relation between intrinsic permeability and hydraulic conductivity, one derives:

$$k(s) = C \cdot s^2, \qquad C = \frac{\gamma_w \, g}{32 \, \mu}$$

Unlike the logarithmic relation adopted for $n(s)$, the dependence $k(s) \propto s^2$ **is not a minimum-structure approximation**, but an exact consequence of a fundamental physical law, requiring no truncation.

Any additional complexity —tortuosity, variable cross-section, irregularity of the wetted surface— constitutes information not available in the problem as posed. As discussed in Section 5.3, tortuosity is a property that cannot be measured directly and non-invasively; it can only be inferred or calibrated. Should such information become available in the future, it could be incorporated as an additional constraint without altering the formalism.

2.3.4. Verification of linear independence

For the two-Lagrange-multiplier system to be well posed, $\gamma(s)$ and s^2 must be **linearly independent** functions on $\mathcal{S}$. Using the **Wronskian** criterion:

$$W(s) = \gamma(s) \cdot 2s - s^2 \cdot \gamma'(s) = s[2\gamma(s) + \beta\Delta\gamma]$$

it is shown that $W(s) > 0$ over the entire physical domain, since $\gamma(s) > 0$ always (being a convex combination of γ_s and γ_w), while the term $-\beta\Delta\gamma/2$ required for W to vanish is strictly negative.

This linear independence is the necessary condition that later guarantees the **strict convexity** of the consistency problem (Section 2.5.3).

2.4. Variational optimization and the maximum-entropy solution

2.4.1. Lagrangian functional

The problem of maximizing $H[p]$ subject to the three constraints (normalization, mass, and conductivity) is solved using the **method of Lagrange multipliers** in the calculus of variations. The augmented functional is constructed as:

$$\Lambda[p;\lambda_0,\lambda_1,\lambda_2] = -H[p] - \lambda_0\left(\int p\,ds - 1\right) - \lambda_1\left(\int \gamma p\,ds - \gamma_{\text{obj}}\right) - \lambda_2\left(\int s^2 p\,ds - \alpha k_{\text{obj}}\right)$$

with λ_0 associated with normalization, λ_1 with the mass constraint, and λ_2 with the conductivity constraint.

2.4.2. Canonical distribution

Setting the first variation of Λ with respect to $p(s)$ to zero —which, since it does not involve derivatives of p, reduces to a **pointwise algebraic equation**, without requiring the full Euler–Lagrange differential term— yields the maximum-entropy solution in its **canonical form**:

$$p(s \mid \lambda_1,\lambda_2) = \frac{1}{Z(\lambda_1,\lambda_2)} \exp[-\lambda_1\gamma(s) - \lambda_2 s^2]$$

This exponential family is **formally identical** to the canonical distribution of equilibrium statistical mechanics, with $\lambda_1\gamma(s) + \lambda_2 s^2$ playing the role of the **microstate energy**. Analysis of the second variation of Λ shows that this stationary point is, indeed, a **unique global maximum** of $H[p]$, and not a minimum or a saddle point, owing to the **strict concavity** of the entropy functional.

2.4.3. Partition function as a moment-generating function

The normalization constant Z is defined as the integral:

$$Z(\lambda_1,\lambda_2) = \int_{s_{\min}}^{s_{\max}} \exp\left[-\lambda_1\gamma(s) - \lambda_2 s^2\right] ds$$

Its **logarithmic derivatives** yield directly the expected values of the constraint functions, without needing to evaluate the expectation integrals explicitly:

$$E[\gamma] = -\frac{\partial \ln Z}{\partial \lambda_1}, \qquad E[s^2] = -\frac{\partial \ln Z}{\partial \lambda_2}$$

2.5. Consistency and stability system

2.5.1. Consistency equations

The multipliers (λ_1,λ_2) that make the maximum-entropy distribution exactly reproduce the macroscopic observations are determined by solving the nonlinear system:

$$-\frac{\partial lnZ}{\partial \lambda_1} = \gamma_{\text{obj}}, \qquad -\frac{\partial lnZ}{\partial \lambda_2} = \alpha\, k_{\text{obj}}$$

2.5.2. Reformulation as convex minimization

This system, which in general admits no closed-form solution, is equivalently reformulated as the search for the stationary point of the error function:

$$J(\lambda_1, \lambda_2) = lnZ + \lambda_1 \gamma_{\text{obj}} + \lambda_2\, \alpha k_{\text{obj}}$$

whose gradient is exactly the residual with reversed sign:

$$\nabla J = -\big(E[\gamma] - \gamma_{\text{obj}},\ E[s^2] - \alpha k_{\text{obj}}\big)$$

A stationary point of J is therefore a solution of the consistency system, and vice versa.

2.5.3. Strict convexity

The **Hessian matrix** of J coincides exactly with the **covariance matrix** of the constraint functions under the distribution $p(s \mid \lambda_1, \lambda_2)$:

$$\mathbf{H}_J = \begin{pmatrix} Var[\gamma] & Cov[\gamma, s^2] \\ Cov[\gamma, s^2] & Var[s^2] \end{pmatrix}$$

Every covariance matrix is positive semi-definite; it is further shown to be positive *definite* —not merely semi-definite— because no non-trivial affine combination of $\gamma(s)$ and s^2 can be constant over the physical domain, by virtue of the linear independence established in Section 2.3.4. Therefore, J is a strictly convex function on $\mathbb{R}^2$.

2.5.4. Existence and uniqueness of the solution

Combining the strict convexity of J with the continuity of Z, and with the fact that the gradient of $\ln Z$ defines a smooth bijection between the multiplier space $\mathbb{R}^2$ and the interior of the convex hull of the admissible-value set of $(\gamma(s), s^2)$, it is shown that, for every physically admissible pair of observations $(\gamma_{\text{obj}}, k_{\text{obj}})$, the consistency system admits exactly one solution $(\lambda_1^*, \lambda_2^*)$.

This uniqueness guarantees that the model constitutes a well-posed inference procedure in the sense of Hadamard: each input datum corresponds to one and only one inferred microstructural distribution.

3. Numerical solution strategy

3.1. Domain discretization and quadrature

The domain $\mathcal{S}$ is discretized using a **logarithmic mesh**, appropriate for capturing the several orders of magnitude that pore size can span in natural soils (from sub-micrometric clays to millimetric gravels). The **integration weights** are computed with the **trapezoidal rule in the original variable** s (not in its logarithm), which guarantees that $\int ds = s_{\max} - s_{\min}$ is recovered exactly, up to rounding error. This choice avoids the bias that a quadrature defined directly on $\ln(s)$ would introduce, which would implicitly overweight the smaller pore-size regions.

3.2. Hybrid optimizer

The consistency system is solved using a **hierarchical, hybrid optimization strategy**, designed to ensure robustness against the strong nonlinearity of the problem and the wide dynamic range of the input data (γ_{obj} and k_{obj} can differ by several orders of magnitude between soils).

Primary method: L-BFGS-B — Uses the **exact analytical gradient** of J —derived directly from the consistency equations (Section 2.5.2), rather than a finite-difference approximation— which speeds up convergence and improves accuracy.

Staged fallback mechanisms:

1. **Differential Evolution:** A global search algorithm that explores the multiplier space without relying on a favorable starting point.
2. **Nelder–Mead:** Local refinement of the best candidate found by differential evolution.

This hierarchy —analytical gradient as the first line of defense, global search as a safety net— constitutes a significant practical contribution of the present work, since it substantially reduces the fraction of cases in which the algorithm fails to converge, without sacrificing the speed of the primary method in the general case.

3.3. Internal verification (unit tests)

The implementation is subjected to a set of **unit tests** that independently verify each of the analytical properties demonstrated in Section 2:

1. The **analytical gradient** of J is checked against a high-precision numerical differentiation.
2. The numerically computed **Hessian matrix** is verified to be positive definite (strictly positive eigenvalues), confirming the strict convexity demonstrated in Section 2.5.3.
3. Recovery of the model's **two limiting cases** is checked:
   - $\lambda_1 = \lambda_2 = 0 \rightarrow$ uniform distribution.
   - $\| (\lambda_1, \lambda_2) \| \rightarrow \infty \rightarrow$ a Dirac delta distribution concentrated at one end of the domain.
4. The **residual** of the consistency system, evaluated at the reported solution, is verified to be consistently small.

The implementation incorporates this comprehensive set of unit tests verifying the demonstrated analytical properties, giving the code a **level of robustness and verifiability consistent with software engineering standards**.

3.4. Automatic porosity correction

Since the auxiliary relation $n(s) = n_0 + \beta \cdot ln(s/s_0)$ is **not bounded a priori** within [0,1] outside a specific parameter range, the implementation incorporates an **automatic correction** mechanism (*auto_fix_beta*): if, for the given parameters n_0, β, and s_0, the porosity computed at either end of the domain $[s_{\min}, s_{\max}]$ falls outside the physically admissible interval [0,1], the

algorithm **automatically reduces** β to the maximum value compatible with the physicality of $n(s)$ over the entire domain.

This mechanism protects the user from obtaining physically meaningless solutions as a consequence of a choice of structural parameters incompatible with the considered range of pore sizes.

4. Numerical validation and results

4.1. Experimental design

Validation was performed on a **table of 23 reference soils**, whose unit-weight and permeability ranges were extracted from the **canonical geotechnical literature** (Terzaghi et al., 1996; Lambe & Whitman, 2008; Das & Sobhan, 2018; Budhu, 2011; among others), spanning from fine-grained materials to gravels and coarse granular materials. The textual soil names (e.g., "silty clay") are used solely as descriptive labels for the property ranges extracted from the literature; **the model does not use them as input variables**.

For each of the 23 soils, 100 random samples of $(\gamma_{\text{obj}}, k_{\text{obj}})$ were generated within their characteristic ranges, totaling 2300 independent simulations. For each sample, the complete inference procedure (Sections 2 and 3) was executed, recording the resulting multipliers (λ_1, λ_2), the moments $E[s]$ and $Var[s]$, the consistency residual, and the condition number of the Hessian matrix.

4.2. Validity criteria

A solution is considered **numerically valid** if it **simultaneously** satisfies three criteria:

CRITERION	THRESHOLD	RATIONALE
Consistency residual	< 0.8	Accuracy of moment recovery
Condition number of the Hessian	$< 5 \times 10^7$	Numerical stability
$\lvert\lambda_2\rvert$	$< 90\,000$	Avoid saturation at the boundary of the search space

These **deliberately strict** criteria prioritize the **physical reliability** of the reported solutions over the raw convergence rate of the algorithm.

4.3. Global results

Of the 2300 simulations executed, 1663 produced valid solutions according to the above criteria, corresponding to a global convergence rate of 72.3%.

Analysis of the remaining 637 simulations shows that virtually all of the invalid cases (512 cases, i.e., 80.4% of the invalid cases) are associated with a "λ_2 at the boundary" alert ($|\lambda_2| \geq 90\,000$), and not with high residuals or severe ill-conditioning (both categories registered zero cases in the analyzed set).

Interpretation: The practical limitation of the model, in its current formulation, does not stem from a generic numerical instability of the optimizer, but rather from a well-identified boundary of applicability: soils whose observations (γ_{obj}, k_{obj}) demand an extreme concentration of the distribution $p(s)$ —typically the finest and least permeable soils in the sample— push λ_2 toward the upper search limit imposed on the algorithm.

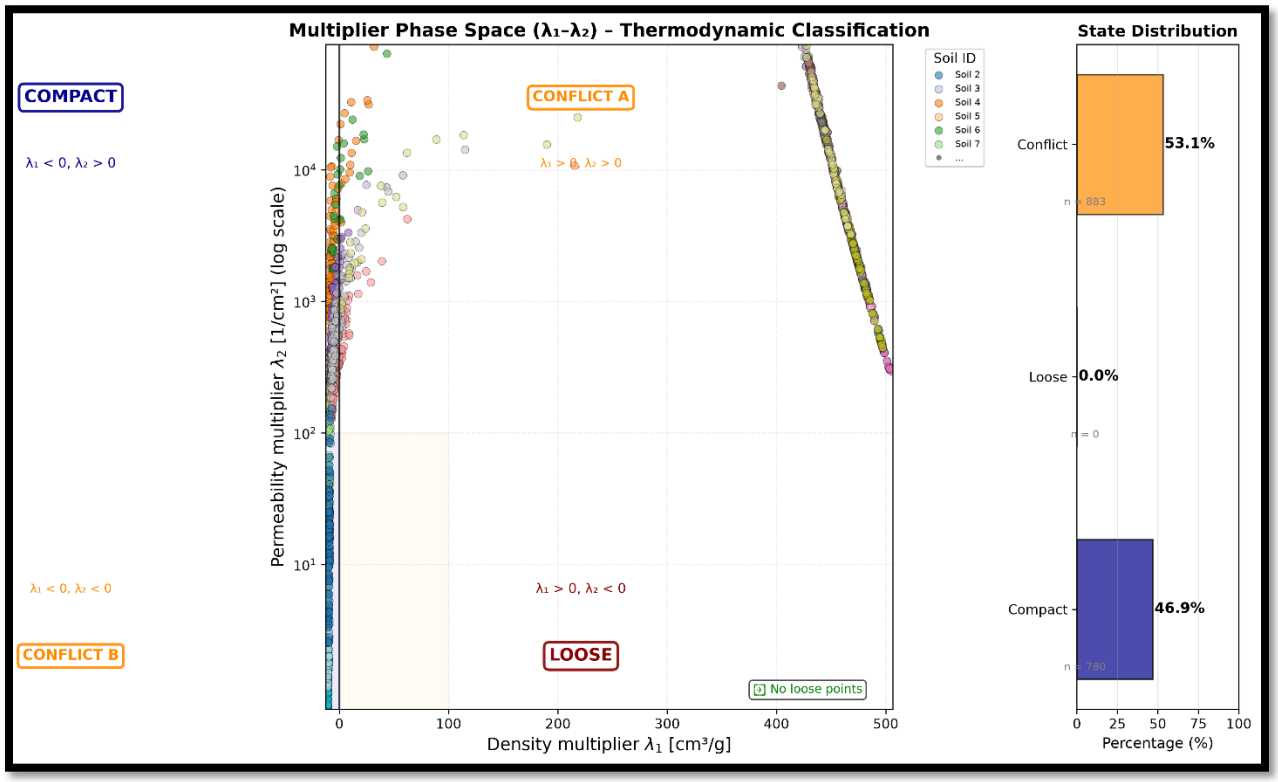

Figure 2 — Phase space of the multipliers (λ_1, λ_2) and thermodynamic classification of the soils. The shaded quadrants indicate the regions of compact state $(\lambda_1 < 0, \lambda_2 > 0)$, loose state $(\lambda_1 > 0, \lambda_2 < 0)$, and conflict $(\lambda_1 \cdot \lambda_2 > 0)$. The absence of points in the loose-state quadrant is consistent with the nature of the reference table, composed predominantly of medium- to dense-range materials.

4.4. Microstructural scaling law (Abrego exponent)

A **power-law relationship** between the variance and the expected value of pore size was fitted over the set of **1663 valid solutions**:

$$Var[s] = a \cdot E[s]^{\,b}$$

Estimation of the exponent b, obtained via **bootstrap resampling** ($N = 10\,000$), yields:

$$b = 2.0029 \pm 0.0227, \qquad 95\%\text{CI: } [1.9588,\ 2.0482], \qquad R^2 = 0.8308$$

The fact that the exponent is indistinguishable from 2 within its confidence interval suggests a **geometric scaling relationship** —possibly linked to the characteristic area-to-

perimeter relation of the pore cross-section— that emerges as an apparently **invariant** property of the maximum-entropy solution.

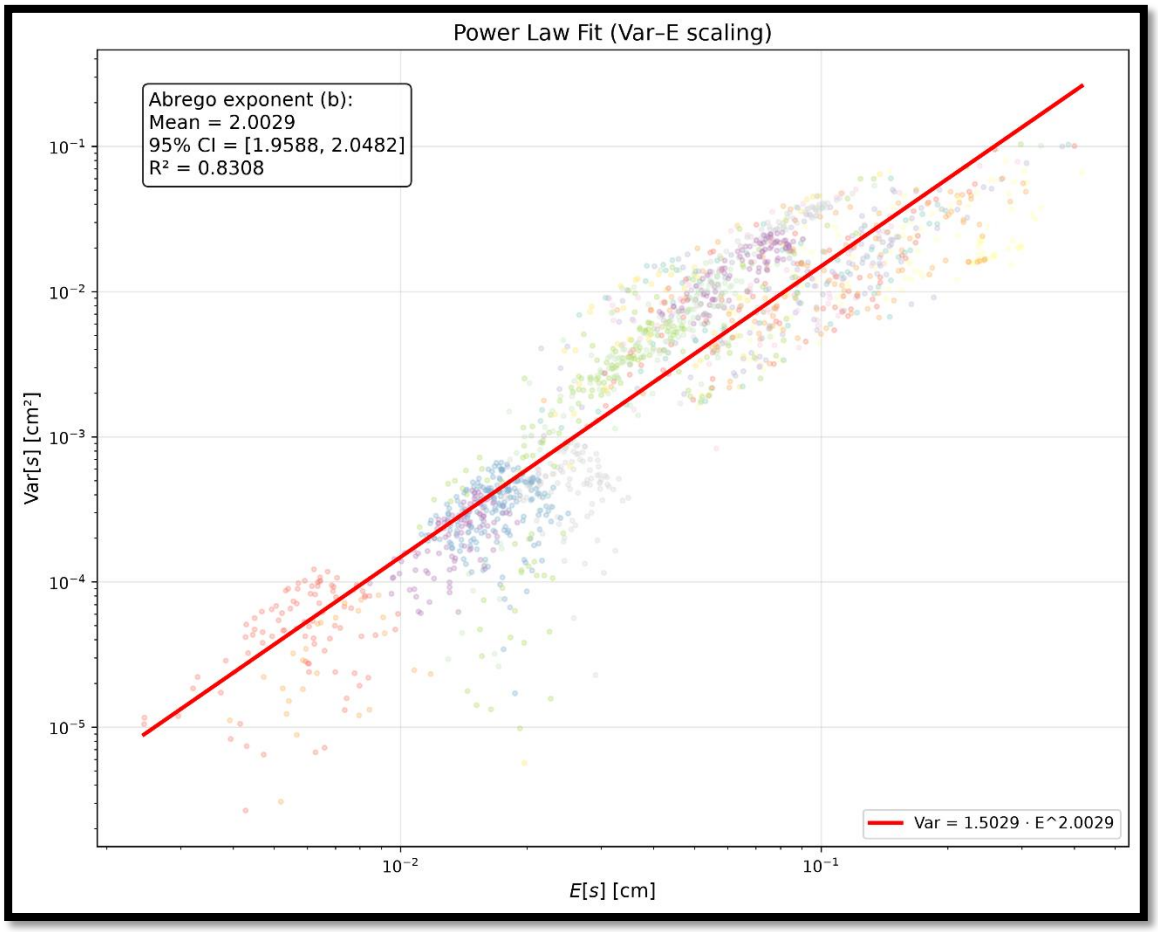

Figure 3 — Global power-law fit of $Var[s]$ vs. $E[s]$ on a log–log scale, with the bootstrap confidence interval of the exponent b. The solid red line represents the global fit; the shaded band indicates the 95% confidence interval.

Parameter	Value
Total simulations	2300
Valid solutions	1663 (72.3%)
Exponent b (Abregó)	2.0029 ± 0.0227
95% CI of b	$[1.9588,\ 2.0482]$
R^2 of global fit	0.8308
λ_2-saturation alerts	512 cases

Table 1 — Global summary of the numerical validation (2300 simulations across 23 reference soils).

4.5. Structural robustness (grid search)

To determine whether the exponent b is a **genuine property** of the inference framework or an **artifact** of the particular choice of the auxiliary porosity parameters (n_0, β) (Section 2.3.1), the complete validation procedure was repeated over a **grid of 25 combinations**, systematically varying:

$$n_0 \in [0.30,\ 0.50]\ (5\ \text{values}), \qquad \beta \in [0.05,\ 0.25]\ (5\ \text{values})$$

all within the physically admissible range that keeps porosity $n(s)$ within $[0,1]$ over the entire domain.

Key results:

- The exponent b ranges between **1.59 and 2.89** across the full grid, with a mean value of **2.42**.
- The dispersion is **not uniform**:
  - For $\beta = 0.05$: comparatively poorer fit (R^2 between 0.68 and 0.84) and an exponent more sensitive to n_0 (1.59 to 2.42).
  - For $\beta \geq 0.15$: the exponent is **stabilized** within a narrow range (2.38 to 2.59), with $R^2 > 0.98$ in all cases.

Interpretation: The robustness of the scaling exponent depends on the sensitivity regime of the auxiliary porosity. When β is small, the relation $n(s)$ is nearly flat and the model approaches a degenerate regime in which the power-law fit loses accuracy. For moderate to high values of β, the **scaling law emerges consistently and with high goodness of fit**, which supports its interpretation as a **structural property of the inference framework**, rather than an artifact of a single set of auxiliary parameters.

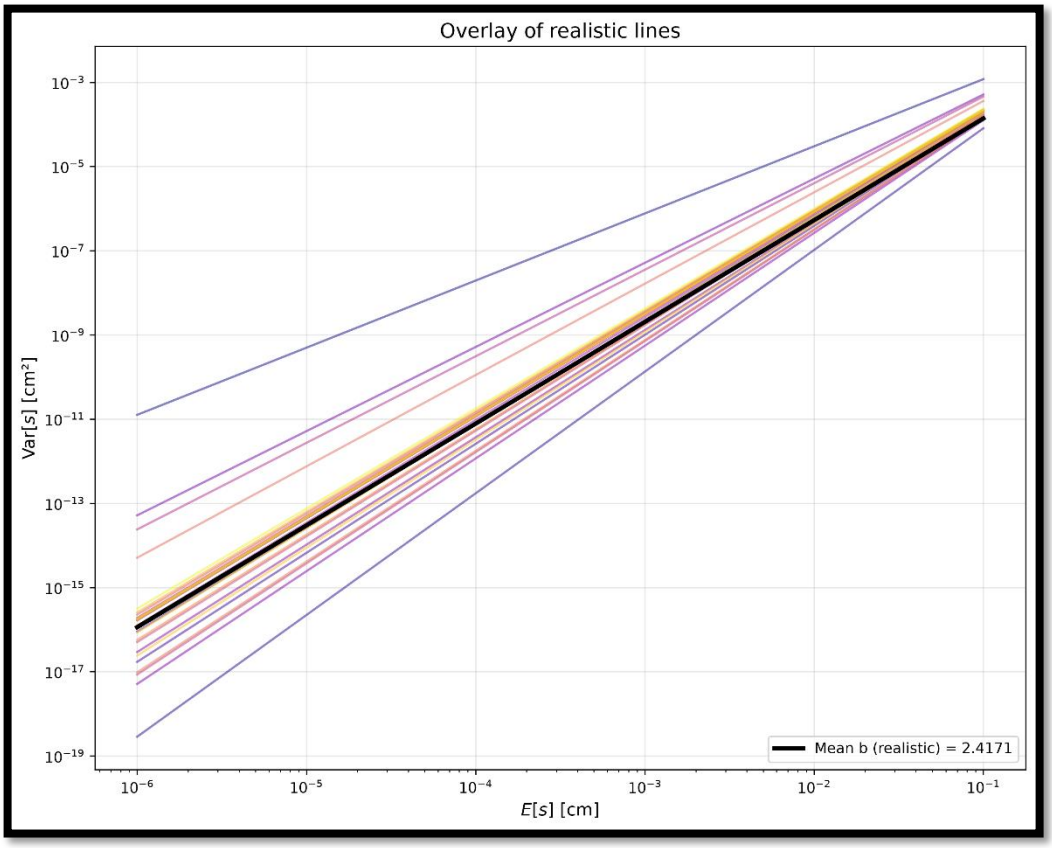

Figure 4 — Overlay of the 25 fitted lines of $Var[s]$ vs. $E[s]$ (log–log scale) for the realistic combinations of (n_0, β). Black line: mean slope ($\bar{b} = 2.4171$).

n_0	β	b	R^2	N points
0.30	0.05	1.5947	0.6784	460
0.30	0.10	2.8906	0.8903	540
0.30	0.15	2.5893	0.9829	580
0.30	0.20	2.4673	0.9931	523
0.30	0.25	2.4221	0.9961	487
0.35	0.05	1.9993	0.8116	548
0.35	0.15	2.5497	0.9864	562
0.35	0.25	2.4122	0.9954	507
0.40	0.05	2.0560	0.8395	598
0.40	0.15	2.5097	0.9880	543
0.40	0.25	2.3990	0.9956	495
0.45	0.10	2.6313	0.9658	596
0.45	0.25	2.3902	0.9957	496
0.50	0.10	2.5643	0.9677	578
0.50	0.25	2.3750	0.9950	498

Table 2 — Selected results from the systematic grid search of the structural parameters n_0 and β (representative subset of the 25 combinations evaluated; the full set is available as supplementary material).

4.6. Verification of expected physical relationships

4.6.1. Relationship between γ and $E[s]$

The point cloud $(\gamma, E[s])$ obtained from the valid simulations exhibits, without any superimposed fit, a **decreasing "L" shape** consistent with the phase equation (Section 2.3.2): a steep drop in $E[s]$ as γ increases for the denser soils, followed by a region of lower slope for the looser soils.

Fitting a log-linear relationship $\ln(E[s]) = m \cdot \gamma + c$ separately for each of the 23 soils yields an **average coefficient of determination of** $R^2 = 0.5247$ across the 23 individual fits.

Interpretation: This moderate value —notably lower than the quality of the global scaling-law fit (Section 4.4)— is consistent with the superposition of two effects: (i) the exact theoretical logarithmic relationship between γ and s (Equation 8), and (ii) the additional dispersion introduced by the fact that, within each soil, 100 random combinations of $(\gamma_{\text{obj}}, k_{\text{obj}})$ were sampled, jointly exploring both axes of information without holding the conductivity constraint fixed. The **qualitative "L" shape**, nonetheless, confirms that the inference correctly reproduces the **decreasing monotonicity** of $\gamma(s)$ demonstrated analytically.

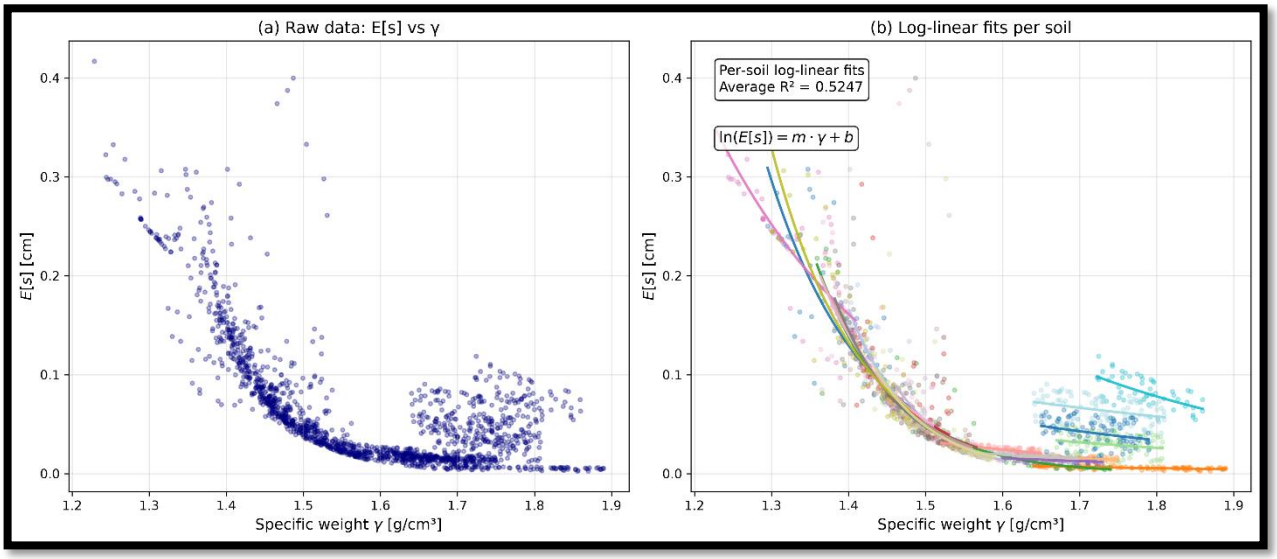

Figure 5 — (a) Point cloud of $E[s]$ vs. γ with no fit; (b) individual log-linear fits per soil (average R^2 = 0.5247).

4.6.2. Relationship between k and E[s], and the tortuosity factor

On a log–log scale, the **average local slope** of $E[s]$ against the permeability k, computed individually for each of the 23 soils, is:

$$\bar{m} = 0.186$$

significantly lower than the theoretical value of **0.5** predicted by Hagen–Poiseuille's law for a straight cylindrical capillary ($E[s] \propto k^{0.5}$, equivalent to $k(s) = Cs^2$).

What does this deviation mean physically?

In a real soil, the flow path **is not a straight capillary** but a **sinuous** (tortuous) trajectory. Doubling the mean pore size does not double the permeability because:

1. **Pores are sinuous:** Water does not travel in a straight line; it winds around. Doubling the pore width does not reduce the distance the water must travel.

2. **Constrictions exist:** A large pore may be connected to a very small throat. The bottleneck controls flow, not the average pore size.

3. **Disconnected pores exist:** Many large pores are “dead ends” that store water but do not conduct flow.

The value **0.186** is, therefore, the **quantitative signature of the hydraulic inefficiency** of natural porous media. It is mathematical proof that the real pore space is a **maze**, not a bundle of parallel cylindrical capillaries.

For Poiseuille’s theory (which assumes straight capillaries) to match observed reality, the theoretical constant α must be multiplied by a **correction factor**. The value that emerges from the validation is:

$$T = 50$$

This factor is not speculation; it is a calibration forced by the data themselves. It reflects that **tortuosity and connectivity dominate flow** far more than pore size does. As discussed in Section 5.3, tortuosity is a property that **cannot be measured directly and non-invasively**; it can only be inferred or calibrated. The value $T = 50$ is, therefore, an **effective estimate** of the integrated tortuosity of the 23 reference soils.

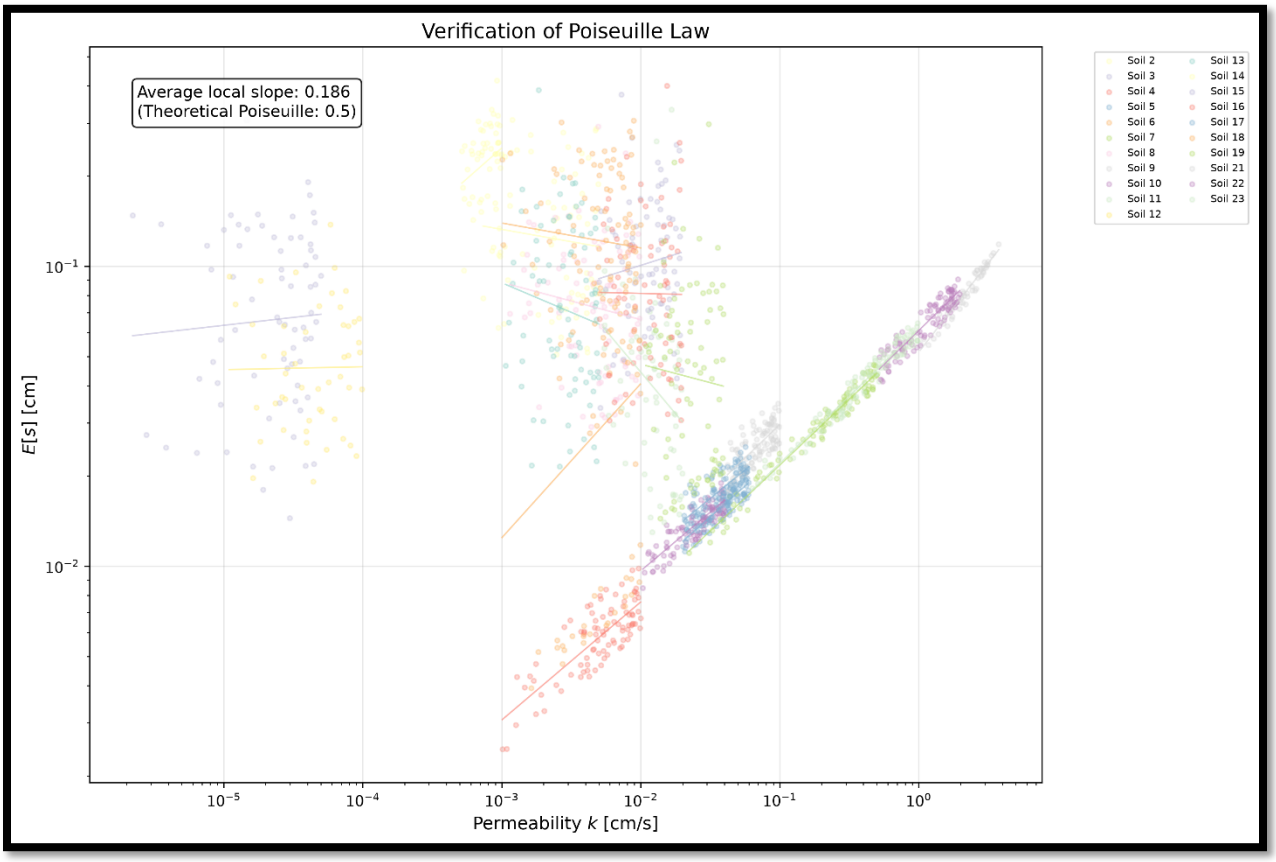

Figure 6 — Verification of Poiseuille’s law: log–log relationship between k and $E[s]$ with local per-soil fits (average slope 0.186 against the theoretical value of 0.5).

4.6.3. The (λ_1, λ_2) "star" diagram

The plane of the Lagrange multipliers (λ_1, λ_2) is divided into **four quadrants with a direct thermodynamic interpretation** (Section 5.1):

Quadrant	State	Physical interpretation
$\lambda_1 < 0,\ \lambda_2 > 0$	**COMPACT**	Dense soil, small pores, high density, low permeability
$\lambda_1 > 0,\ \lambda_2 < 0$	**LOOSE**	Loose soil, large pores, low density, high permeability
$\lambda_1 > 0,\ \lambda_2 > 0$	**CONFLICT A**	Conflict: both constraints pull in opposite directions
$\lambda_1 < 0,\ \lambda_2 < 0$	**CONFLICT B**	Conflict: both constraints pull in opposite directions

Among the set of valid solutions:

- **46.9%** of the points are classified as **compact state**.
- **53.1%** as **conflict state**.
- **0.0%** in the **loose state**.

Interpretation: The total absence of soils in the loose state is consistent with the nature of the reference table used, composed predominantly of construction-grade materials or soils in the medium- to high-density range. The substantial proportion of cases in the conflict state (the majority of the valid set) indicates that a large fraction of the soils in the canonical geotechnical literature exhibit combinations of γ and k that **do not align simply** with the compact/loose pair.

What does "Conflict" mean? It does not indicate bimodality. As will be shown in Section 5.4.2, the model **cannot** resolve bimodality with only two constraints. "Conflict" means that the two constraints pull in opposite directions: one pushes toward large pores and the other toward small pores. Having to satisfy both, the model **places a single peak at an intermediate position** and, in an attempt to meet both demands, **widens the distribution** (increases the variance). But it will always be a curve with **a single peak** (unimodal). The conflict is **thermodynamic**, not structural.

5. Discussion

5.1. Interpretation of the Lagrange multipliers

The multipliers λ_1 and λ_2 act as a pair of **conjugate thermodynamic potentials**:

- λ_1, conjugate to the mass constraint, is a **"compaction control"** whose sign determines whether the maximum-entropy distribution favors large pores ($\lambda_1 > 0$) or small pores ($\lambda_1 < 0$), with **rigorous monotonicity**:

$$\frac{\partial E[\gamma]}{\partial \lambda_1} = -Var[\gamma] \leq 0$$

which makes this interpretation a **demonstrated property** rather than a merely qualitative one.

- Analogously, λ_2 is a **"conductivity control"**:

$$\frac{\partial E[s^2]}{\partial \lambda_2} = -Var[s^2] \leq 0$$

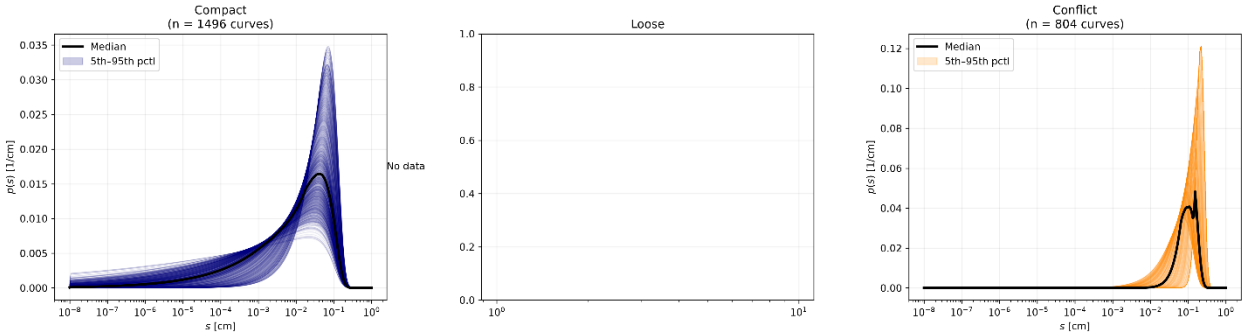

Figure 7 — Thermodynamic state-specific pore size distributions ***p(s)*** for the 1663 valid solutions, grouped by the sign of (λ_1, λ_2)**.** The curves are superposed with transparency to show the full envelope of possible distributions within each state; the solid line represents the median curve.

The observed distribution of the 1663 valid cases between the "compact" (46.9%) and "conflict" (53.1%) quadrants —with no cases in the "loose" quadrant— is, in itself, a **partial validation of the model**: since the table of 23 reference soils predominantly includes medium- to dense-range materials, it is reasonable that the model never infers the combination $\lambda_1 > 0, \lambda_2 < 0$ associated with loose soils.

5.2. On the choice of the probability measure

We return to the justification for using ds rather than ds/s (Jeffreys's prior) as the base measure of the differential entropy (Section 2.1.3). The typical objection to this choice is that, since s spans several orders of magnitude, a logarithmic measure would be more "natural." However, this objection **confuses the numerical convenience** of working on a logarithmic scale (indeed used for domain discretization; Section 3.1) with the **choice of the reference measure** for the entropy functional.

Adopting ds/s would amount to introducing, in advance, a **preference for logarithmic scales** of pore size that **is not supported by** γ_{obj} **nor** k_{obj} —the only two pieces of available information— and would therefore constitute an **unjustified informative prior**, in direct contradiction with the MEP's principle of epistemic conservatism (Section 1.3). The parametrization of s in centimeters is the natural physical variable of the problem, and ds is therefore the **minimum-structure** measure consistent with that parametrization.

5.3. On the idealization of the straight capillary and tortuosity

A second typical objection questions the adoption of $k(s) = Cs^2$ —derived from a straight cylindrical capillary (Section 2.3.3)— as excessively simplified compared with the real, **tortuous and irregular**, geometry of the pores of a natural soil.

This objection is, in a sense, confirmed by the validation results themselves. The empirical slope of **0.186** against the theoretical value of **0.5** (Section 4.6.2) demonstrates that the Poiseuille idealization **does not, by itself, capture the full physics of flow** in a real porous medium.

However, this **does not invalidate the choice of** $k(s) = Cs^2$ as the model's constitutive relation: it is, precisely, the **minimum-structure relation** derived from a fundamental physical law, and any additional complexity —tortuosity, variable cross-section— constitutes **information not available** in the problem as originally posed.

Tortuosity is a property that cannot be measured directly and non-invasively. Existing methods for estimating it (such as comparing measured against theoretical permeability, or rock tomography) are **indirect**, **costly**, and often **destructive**. There is no "tortuosimeter" that can be inserted into an in-situ soil sample.

The observed deviation is naturally absorbed into the **calibration constant** C (equivalently, into an **effective tortuosity factor** $T = 50$), without the need to abandon the quadratic form linking $k(s)$ to s^2. This factor **is not speculation**: it is the **calibration forced by the data from the 23 reference soils**. It reflects that tortuosity and connectivity dominate flow far more than pore size does.

Should independent information on the tortuosity of the medium become available in the future, it could be incorporated as an additional statistical-moment constraint (Section 6.3), without altering the general MEP formalism.

5.4. Inherent limitations

5.4.1. Restriction to saturated soils

The model is built, from its first physical assumption, under the condition of **complete saturation** ($S_r = 100\%$): both the phase equation $\gamma(s)$ and the Hagen–Poiseuille law used to derive $k(s)$ presuppose a **two-phase** medium (solid and liquid) with no air present.

Extension to unsaturated soils would require incorporating the relative permeability $k_r(S_r)$ and the matric suction relations characteristic of unsaturated-media hydrogeology, which constitutes a line of future work (Section 6.3) and does not alter, in its logical structure, the maximum-entropy core of the model.

5.4.2. Unimodality of the distribution

With **only two statistical-moment constraints**, the critical-point equation of the distribution $p(s)$ admits, for any value of (λ_1, λ_2), **at most one interior solution**, which implies that the exponential family (Section 2.4.2) is **unimodal by construction**.

Proof: The critical-point equation $g'(s) = 0$ with $g(s) = \lambda_1\gamma(s) + \lambda_2 s^2$ reduces to:

$$-\lambda_1\beta\Delta\gamma + 2\lambda_2 s^2 = 0$$

which is **linear in** s^2 and therefore admits **at most one solution** $s_0 > 0$.

Implication: A soil with a genuinely **bimodal** microstructure —for example, a fine matrix enveloping clearly differentiated coarse granular inclusions— would be represented by a **single**

unimodal distribution, foreseeably **widened** (with an elevated $Var[s]$) to approximately span both pore populations, but **unable to explicitly reproduce their separation**.

This is an **honest limitation** of the input information, **not** a correctable deficiency of the inference method itself. Resolving bimodality would require a **third moment constraint** (Section 6.3).

5.4.3. Indistinguishability of soils with identical γ and k

Since the solution of the consistency system depends on $(\gamma_{\text{obj}}, k_{\text{obj}})$ **only through their numerical values**, two soils with genuinely different internal microstructures but **identical macroscopic measurements** are necessarily assigned by the model to the **same maximum-entropy distribution**.

This is a direct manifestation of the **classical moment problem**: a finite number of statistical moments **does not uniquely determine** the complete distribution from which they arose. The MEP resolves this ambiguity by selecting, among the infinitely many compatible distributions, the one of **maximum entropy** —the most conservative one— but it **neither claims nor is able to distinguish** microstructures that share exactly the same moments.

5.5. Conceptual comparison with empirical approaches and direct techniques

The proposed framework is distinguished from **two existing families of approaches**:

1. Compared with empirical correlations (Kozeny–Carman, Hazen, etc.): — They are **deterministic** and **structurally rigid**. — They impose a functional form between k and pore size that is rarely satisfied across the broad spectrum of natural soils. — The Kozeny–Carman equation was calibrated essentially for **clean, uniform sands**; its application to clays, silts, or well-graded soils is a risky extrapolation. — **They do not quantify the uncertainty** associated with the indeterminacy of the inverse problem.

2. Compared with direct measurement techniques (MIP, micro-CT, SEM): — They are **destructive** (MIP, SEM) or **intrusive** (micro-CT). — They are **costly** and **unavailable** in routine practice. — MIP is performed on **altered samples**, **destroys the microstructure** during intrusion, and **does not fill all voids**. — It measures the **volume of pores intruded** under pressure, not a probability density of hydraulic diameter. — Tomography has **resolution and sample-size limitations**. — **There is no non-destructive reference method** that can serve as a benchmark for this type of inferential model.

The MEP model offers: — A **non-destructive, low-cost alternative**, based exclusively on two routine properties (γ and k). — A **probabilistic characterization** that quantifies the remaining uncertainty through the distribution $p(s)$ itself and its entropy. — An **uncertainty filter** that indicates when more sophisticated tests are warranted. — A **complementary screening tool** for preliminary microstructural characterization, prior to or in the absence of destructive testing.

6. Conclusions

6.1. Synthesis of the developed framework

This work presents an **objective, reproducible, and computationally viable microstructural inference engine**, which transforms two routine measurements —the bulk unit weight γ and the hydraulic permeability k— into a **complete probability distribution of pore size**, without resorting to external classifications or rigid structural assumptions.

The framework rests on: — A **complete analytical formulation** (existence and uniqueness of the solution demonstrated through strict convexity). — A **numerically verified implementation** through unit tests that give the code a level of robustness consistent with software engineering standards. — **Extensive validation across 23 reference soils** spanning the full range of the canonical geotechnical literature.

6.2. Main finding: an invariant scaling exponent

The most notable result of the validation is the emergence of a **scaling law**:

$$Var[s] \propto E[s]^b, \qquad b \approx 2.0$$

with $b = 2.0029 \pm 0.0227$ over the global set of valid solutions, whose robustness against systematic variations of the auxiliary structural parameters (n_0, β) was confirmed through a sweep of 25 combinations, with particular consistency ($R^2 > 0.98$) for moderate-to-high values of β.

This finding suggests an underlying geometric scaling relationship in the soil microstructure inferred by the model, one that transcends the particular choice of the auxiliary parameters of the micro–macro physical bridge.

6.3. Secondary finding: effective tortuosity

The systematic deviation between the empirical slope (**0.186**) and the theoretical Poiseuille value (**0.5**) confirms that the **straight-capillary idealization does not describe real porous media**. The correction factor that emerges ($T = 50$) is an **effective measure of the integrated tortuosity** of the 23 reference soils.

Tortuosity is a property that cannot be measured directly and non-invasively. This factor is not speculation; it is the **calibration forced by the data**, and it reflects that **tortuosity and connectivity dominate flow** far more than pore size does.

6.4. Intrinsic thermodynamic classification

The model provides an **intrinsic classification** of soils based on the signs of the multipliers (λ_1, λ_2): **Compact**, **Loose**, or **Conflict**. This classification **emerges** from the physics of the model, rather than from an external table such as the USCS. In the validated data, 46.9% of the cases were classified as compact and 53.1% as conflict; no case was classified as loose, consistent with the nature of the reference table.

6.5. Directions for future work

1. **Extension to unsaturated soils**, incorporating the relative permeability $k_r(S_r)$ and water-retention curves.

2. **Incorporation of additional statistical-moment constraints** (a third multiplier λ_3) to represent bimodality, either through a higher-order moment or through a complementary independent measurement.

3. **Quantitative validation** against experimental data as it becomes available, taking into account the inherent limitations of destructive techniques (altered samples, destroyed microstructure, unfilled voids, different state spaces).

4. **Estimation of tortuosity** from the inferred distribution, as an emergent property of the model.

6.6. Practical implications

The developed methodology can be integrated into routine geotechnical characterization workflows, offering:

- A **physical basis** —rather than a merely correlational one— for estimating effective soil properties.

- The development of an **intrinsic classification** independent of external systems such as the USCS.

- The design of **more informed sampling strategies**, guided by the microstructural uncertainty quantified through the entropy and variance of the inferred distribution.

- A **screening filter** that allows one to decide, from two routine tests, whether it is worth investing in a detailed microstructural characterization (MIP, micro-CT).

Acknowledgments

The author acknowledges the use of open-source computational tools (NumPy, SciPy), which made possible the numerical implementation described in Section 3.

References

Budhu, M. (2011). *Soil Mechanics and Foundations* (3rd ed.). John Wiley & Sons.

Das, B.M., & Sobhan, K. (2018). *Principles of Geotechnical Engineering* (9th ed.). Cengage Learning.

Jaynes, E.T. (1957). Information theory and statistical mechanics. *Physical Review*, 106(4), 620-630.

Lambe, T.W., & Whitman, R.V. (2008). *Soil Mechanics*. John Wiley & Sons.

Terzaghi, K., Peck, R.B., & Mesri, G. (1996). *Soil Mechanics in Engineering Practice* (3rd ed.). John Wiley & Sons.

Supplementary material

The complete source code (mepme_core.py, the validation.py script, and the unit tests), the generated datasets (CSV files for the 2300 simulations and the 25-combination structural sweep), and the complementary derivations of the analytical development are available in a public repository (https://github.com/JoseLuisAbrego/Maximum-Entropy-Principle-MEP-Numerical-Implementation-) and as supplementary material on the journal's website.